An ancient metal-poor population in M32, and halo satellite accretion in M31, identified by RR Lyrae stars[★]

Ata Sarajedini,[1]† S.-C. Yang,[1,2] A. Monachesi,[3] Tod R. Lauer[4] and S. C. Trager[5]

[1]*Department of Astronomy, University of Florida, 211 Bryant Space Science Center, Gainesville, FL 32611, USA*
[2]*Korea Astronomy & Space Science Institute, Daejeon 305-348, Korea*
[3]*Department of Astronomy, University of Michigan, 830 Dennison Building, 500 Church Street, Ann Arbor, MI 48109, USA*
[4]*National Optical Astronomy Observatory, PO Box 26732, Tucson, AZ 85726, USA*
[5]*Kapteyn Astronomical Institute, PO Box 800, 9700 AV Groningen, the Netherlands*

ABSTRACT

We present time series photometry of two fields near M32 using archival observations from the Advanced Camera for Surveys Wide Field Channel on-board the *Hubble Space Telescope*. One field is centred about 2 arcmin from M32, while the other is located 15 arcmin to the south-east of M31. The imaging covers a time baseline sufficient for the identification and characterization of a total number of 1139 RR Lyrae variables of which 821 are ab-type and 318 are c-type. In the field near M32, we find a radial gradient in the density of RR Lyraes relative to the centre of M32. This gradient is consistent with the surface brightness profile of M32, suggesting that a significant number of the RR Lyraes in this region belong to M32. This provides further confirmation that M32 contains an ancient stellar population formed around the same time as the oldest population in M31 and the Milky Way. The RR Lyrae stars in M32 exhibit a mean metal abundance of $\langle[\text{Fe/H}]\rangle \approx -1.42 \pm 0.02$, which is ≈ 15 times lower than the metal abundance of the overall M32 stellar population. Moreover, the abundance of RR Lyrae stars normalized to the luminosity of M32 in the field analysed further indicates that the ancient metal-poor population in M32 represents only a very minor component of this galaxy, consistent with the 1–4.5 per cent in mass inferred from the colour–magnitude diagram analysis of Monachesi et al. We also find that the measured reddening of the RR Lyrae stars is consistent with M32 containing little or no dust. In the other field, we find unprecedented evidence for two populations of RR Lyraes in M31 as shown by two distinct sequences among the ab-type variables in the Bailey diagram. When interpreted in terms of metal abundance, one population exhibits a peak at [Fe/H] ≈ -1.3 and the other is at [Fe/H] ≈ -1.9. One possible interpretation of this result is that the more metal-rich population represents the dominant M31 halo, while the metal-poorer group could be a disrupted dwarf satellite galaxy orbiting M31. If true, this represents a further indication that the formation of the M31 spheroid has been significantly influenced by the merger and accretion of dwarf galaxy satellites.

Key words: stars: abundances – stars: Hertzsprung–Russell and colour–magnitude diagrams – stars: variables: RR Lyrae – galaxies: evolution – galaxies: individual: M31, M32.

1 INTRODUCTION

1.1 RR Lyraes and their use in unveiling stellar populations

The class of pulsating stars known as RR Lyrae variables are located at the intersection of the instability strip and the horizontal branch in the Hertzsprung–Russell diagram (Smith 1995). There are three principal types of RR Lyrae variables; those pulsating in the fundamental mode exhibit sawtooth-like light curves and are referred to as ab-type or RR0 variables. The first overtone pulsators generally show sine-curve-shaped light curves, have shorter periods and typically lower amplitudes than the ab-types, and are referred to as c-type or RR1 variables. Lastly, RR Lyraes that pulsate in both the fundamental and first overtone modes (i.e. double mode pulsators) carry the d-type moniker.

The astrophysical utility of RR Lyraes to investigate a number of key questions in the areas of stellar populations and galaxy

formation is well documented. For example, because of their low masses ($\approx 0.7\,\mathrm{M}_\odot$; Smith 1995), the mere presence of RR Lyrae stars in a stellar population suggests an old age ($\gtrsim 10\,\mathrm{Gyr}$) for the system. As such, one does not need to obtain deep photometry beyond the old main-sequence turn-off (MSTO) in order to establish the presence of an old population.

The periods and amplitudes of the ab-type RR Lyrae stars (P_{ab}) are related to their metallicities. Using data on Milky Way field RR Lyraes from Layden (private communication) and those in the Large Magellanic Cloud, Sarajedini et al. (2006) and Alcock et al. (2000), respectively, present relations that correlate the periods and amplitudes of RR Lyraes with their metal abundances. Once the metallicities of the RR Lyraes are determined, their absolute magnitudes can be calculated using relations between [Fe/H] and the absolute magnitude of the RR Lyraes [M_V(RR)], which are then used to estimate the distance to their parent population, be it a star cluster or a galaxy. Lastly, ab-type RR Lyraes are also useful for calculating the line-of-sight reddening. The minimum light colours of these stars are largely independent of their other properties as shown by Guldenschuh et al. (2005) and Kunder, Chaboyer & Layden (2010), making the determination of reddening a simple one-step process.

Thus far, we have presented examples of how RR Lyrae variables can be powerful probes of the systems in which they reside – star clusters or among the field populations of galaxies. It is for this reason that studying them in Local Group galaxies like M31 and M32 provides valuable insights into the properties of these systems.

1.2 RR Lyrae variables in M31

The study of RR Lyraes in M31 has a rich history dating back to the seminal work of Pritchet & van den Bergh (1987) and culminating in the most recent papers by Sarajedini et al. (2009) and Jeffery et al. (2011). Sarajedini et al. (2009, hereafter S09) present *Hubble Space Telescope* (*HST*) Advanced Camera for Surveys (ACS) observations for two fields in the range of 4–6 kpc from the centre of M31. A total of 681 RR Lyraes (555 ab-type and 126 c-type) were identified in the two fields. A mean metal abundance of [Fe/H] $\approx$ -1.5 was determined using the periods and amplitudes of these stars.

The work of Jeffery et al. (2011) is a continuation of the work of Brown et al. (2004) and presents high-quality light curves for RR Lyraes in five fields around M31. These include a halo field at 21 kpc and two halo fields at 35 kpc. In addition, there is a field coincident with one of the streams in the vicinity of M31 and one that covers a disc region about 26 kpc from the centre along the major axis of the galaxy. Besides identifying a number of RR Lyrae variables in these fields, Jeffery et al. (2011) also compare three methods for the determination of RR Lyrae metallicities. We note in passing also that Bernard et al. (2012) present RR Lyraes in two M31 fields along the major axis based on *HST*/ACS observations. These are located in the disc warp and in the outer disc.

1.3 RR Lyrae variables in M32

M32 is an intriguing galaxy, considered to be the prototype of the compact elliptical galaxies. In view of its importance in understanding these objects, its stellar populations have been extensively studied (e.g. Rose 1985; Freedman 1992; Grillmair et al. 1996;

Trager et al. 2000; Worthey 2004; Rose et al. 2005). Recently, using the High Resolution Channel (HRC) on ACS, Monachesi et al. (2011, 2012) have analysed the stellar populations of M32 in a field $\sim$2 arcmin away from its nucleus. They have constructed the deepest optical colour–magnitude diagram (CMD) of M32 ever and derived its star formation history (SFH). They found that M32 has had an extended SFH and is composed of two main dominant populations: a 2–5 Gyr old, metal-rich population and a population older than 5 Gyr, with slightly subsolar metallicity. Their study moreover indicates that a significant contribution from stars older than 10 Gyr is not expected, although there are claims from spectroscopic analysis that such a population should exist in M32 (e.g. Coelho, Mendes de Oliveira & Cid Fernandes 2009). Given the extreme crowding in their field, Monachesi et al. (2011) were unable to detect the oldest MSTO of M32 and thus a census of the oldest stars in M32 is still missing. RR Lyrae stars are therefore a direct indicator of the presence of an ancient population in M32. Alonso-García, Mateo & Worthey (2004) used the Wide Field Planetary Camera 2 (WFPC2) on-board *HST* to image a field $\approx$3.5 arcmin to the east of M32. Comparing the variable star content of this field with that of a control field that samples the M31 field away from M32, they claim to have identified RR Lyraes that belong to M32, although this result remains quite uncertain, since their data suffer from strong photometric and temporal incompleteness. A marginal detection of RR Lyrae stars in M32 was presented by Fiorentino et al. (2010). They used the same HRC field of *HST*/ACS as Monachesi et al. (2011) and identified 17 RR Lyrae variables. Using a Bayesian analysis, they suggest that M32 contains RR Lyrae stars and therefore possesses an old ($\gtrsim$10 Gyr) population. However, the small field of view of ACS/HRC and the strong contamination from M31 make this detection also very uncertain.

As we were preparing this paper, we became aware of the most recent work from Fiorentino et al. (2012), which presents their reduction and analysis of a subset of the data presented herein. They studied the RR Lyraes in the M32 field and investigated their spatial distribution as well as their periods and metallicities. We will highlight their work in more detail within the relevant sections of the present paper, but for the moment, we note that their results are largely in agreement with ours.

1.4 This paper

In the present work, we utilize archival Wide Field Channel (WFC) *HST*/ACS images of two fields in the vicinity of M32 in order to search for RR Lyraes. The ACS/WFC fields have a wider spatial coverage of M32's stellar populations over a range of higher surface brightnesses than the previous WFPC2 and ACS/HRC fields studied. Our primary task is to identify a substantial population of RR Lyraes belonging to M32 that would confirm the presence of a truly ancient, metal-poor population in this galaxy, and characterize their properties so that we can use them to study their parent galaxy. Furthermore, we probe the RR Lyraes in the spheroid of M31 in order to better understand their properties: their metallicities and Oosterhoff types.

The paper is organized as follows. Sections 2 and 3 describe our observations and data reduction including the artificial star experiments we use to characterize our photometric incompleteness. Section 4 provides a description of the techniques used to identify and characterize the RR Lyraes in our sample. We also detail the simulations used to assess any biases present in our variability data. The results and discussion as they pertain to M32 are in Section 5, where we investigate the membership of the RR Lyraes in our field
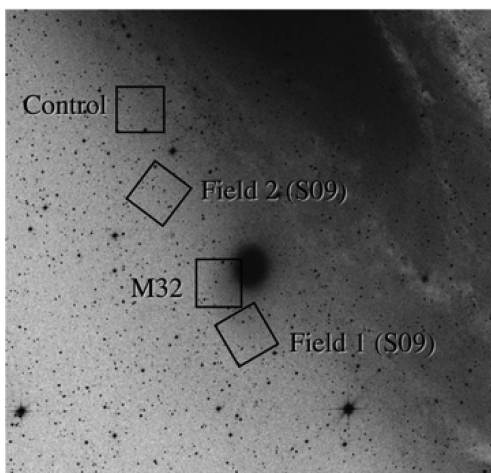
Table 1. Observing log.

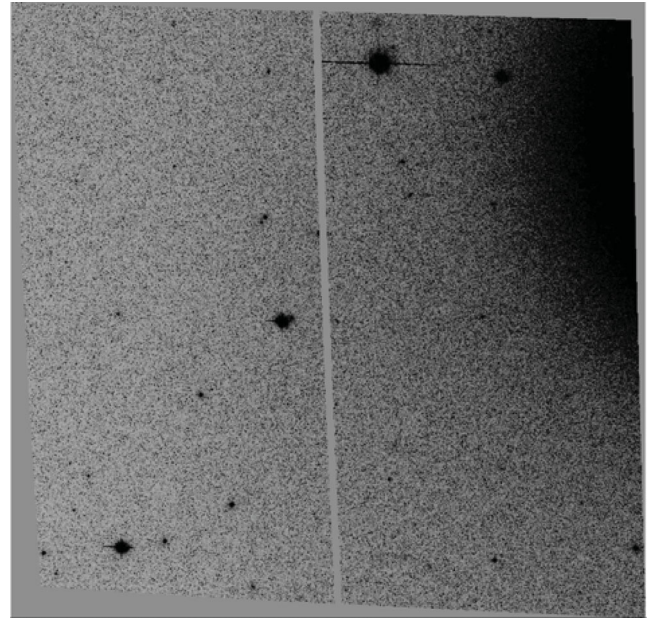| Field	RA (J2000)	Dec. (J2000)	Starting date	Data sets	Filter	Exp time (s)
M32	00 42 55.92	+40 50 50.4	2004 Nov 24	J8F101, J8F103, J8F105	*F606W* *F814W*	2 × 900, 1 × 960, 15 × 1000 1 × 1520, 3 × 1570, 14 × 1580
Control	00 43 28.65	+41 03 43.8	2004 Dec 20	J8F102, J8F104, J8F106	*F606W* *F814W*	2 × 900, 1 × 960, 15 × 1000 1 × 1520, 3 × 1570, 14 × 1580

closest to M32. Section 6 presents the results and discussion of the RR Lyraes that belong to M31, where we show unprecedented evidence for two sequences of ab-type RR Lyraes in the Bailey diagram. Finally, the conclusions of the present work are given in Section 7.
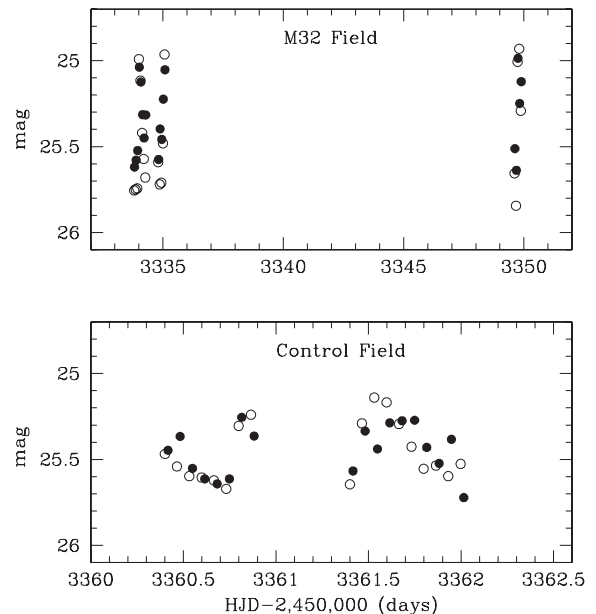
2 OBSERVATIONS

The observations used in the present study were obtained with *HST*/ACS/WFC as part of programme GO-9392 (PI: Mateo). The details of this programme have already been fully described by Rudenko, Worthey & Mateo (2009) and the observing log is shown in Table 1. In summary, two fields were observed; the first one, which we designate 'M32' in Fig. 1, was centred south-east of M32 covering a radial distance range of 1–4.5 arcmin from the centre of M32. Fig. 2 shows a reproduction of the M32 field observed in the *F606W* filter. The second field was meant to be a control field (designated 'Control' in Fig. 1) located roughly 5 arcmin north-east of M32 in order to monitor the M31 background field in the vicinity of M32. The M32 field was observed for a total of ∼5 h in the *F606W* filter and ∼8 h in *F814W*, alternating between the two filters and yielding 18 exposures in each filter. These were taken on 2004 November 24–25 and 2004 December 10. Similarly, the Control field was observed on 2004 December 20–22 for ∼5 and ∼7.5 h in *F606W* and *F814W*, respectively, again alternating between filters and providing 18 exposures per filter. Fig. 3 shows raw unphased light curves for two of our RR Lyrae variables in order to illustrate the cadence of the observations.

Figure 2. The *F606W* filter drizzled ACS image of our M32 field. North is up and east is to the left.

Figure 1. The location of our ACS fields (M32 and Control) along with the two fields from S09 overplotted on a digitized sky survey image in the region of M31. The dwarf elliptical galaxy M32 is near the centre of the image. North is up and east is to the left.

Figure 3. Raw unphased light curves for two of the RR Lyraes in our sample illustrating the cadence of the observations in each field. The filled circles are the *F606W* filter data, while the open circles are in *F814W*.

It is important to note that, as we establish below, the properties of the M31 RR Lyraes in the Control field are significantly different from those in the M32 field. As such, we did not make use of the Control field in the manner it was originally intended – to gauge the level of contamination of M32 stars by the M31 background. Instead, we have determined the background density using selected data from the M32 field as well as the observations presented by S09. Section 5.2 provides more details on the procedure we followed.

3 DATA REDUCTION

3.1 Program frames

The 72 ACS/WFC images were measured using the DAOPHOT/ALLSTAR/ALLFRAME (Stetson 1987, 1994) suite of crowded field photometry programs. The procedure we followed is identical to that used by S09. In summary, once a master coordinate file was constructed for each image and high-precision coordinate transformations between the images established, ALLFRAME was used to fit a high signal-to-noise ratio point spread function to all detected profiles on each of the 36 images in each field. The measurements on each of the individual frames were then matched and only stars appearing on all 36 images were kept.

The standardization procedure of the individual magnitudes is identical to that used by Sarajedini et al. (2006). More specifically, we have made use of the Reiss & Mack (2004) prescription to account for the effects of charge transfer efficiency along with the Sirianni et al. (2005) calibration equations and coefficients to transform our instrumental photometry to the ground-based *VI* system. Each of our magnitude measurements is affected by three sources of systematic error: the uncertainty in the aperture corrections (±0.02 mag), the error in the correction to infinite aperture for the *F*606*W* (±0.00 mag) and *F*814*W* (±0.001 mag) filters, and the error in the ground system *VI* zero-point (±0.05 mag; Sirianni et al. 2005).

3.2 Artificial star experiments

In order to gauge the degree of photometric completeness on our program frames, we have performed a series of artificial star experiments. Beginning with a synthetic CMD generated using IAC-STAR (Aparicio & Gallart 2004) that replicates the appearance of the actual CMD produced from our observations, we selected 50 000 artificial stars. These were placed on the WFC2 images, which is the portion of the field closer to M32, 5000 stars at a time, in a grid pattern with random intrapixel positions. The WFC1 region of the field, which is less crowded than WFC2, received 35 000 artificial stars. The resultant images were photometered using the same procedure as the original images. The overall recovery rates for the artificial stars were 87 per cent for the WFC1 images and 81 per cent for WFC2.

The recovery rates were used to devise a relation between completeness fraction and radial distance from the centre of M32. Since we are interested in correcting the red clump stars and RR Lyraes for photometric incompleteness (see below), we limited this relation to stars in the magnitude range of the horizontal branch.

4 CHARACTERIZATION OF THE VARIABLE STARS AND SIMULATIONS

We use the technique of Yang et al. (2010) and Yang & Sarajedini (2012) to identify and characterize variable stars in the images.

We start by searching all of the variable star candidates located in a range of *V* magnitude (24.5 < *V* < 26). Stars within this *V* magnitude range were evaluated using a reduced χ^2_{VI} defined by the following equation:

$$\chi^2_{VI} = \frac{1}{N_V + N_I} \times \left[\sum_{i=1}^{N_V} \frac{(V_i - \overline{V})^2}{\sigma_i^2} + \sum_{i=1}^{N_I} \frac{(I_i - \overline{I})^2}{\sigma_i^2} \right].$$

Any anomalous data points that deviated from the mean magnitude by ±3σ were excluded from the χ^2_{VI} calculation for each star. Then, we selected only those stars with χ^2_{VI} values greater than 3.0 as potential variable candidates.

The next step involved running our template light-curve fitting routine, RRFIT (Yang & Sarajedini 2012), on the time series photometry of these variable star candidates in order to detect and characterize RR Lyrae stars. RRFIT uses 25 unique light-curve templates (23 RRab-type and two RRc-type variables). It searches over specific period and amplitude ranges and calculates the χ^2 difference between the observed data and each light-curve template. It then determines the optimal light-curve parameters such as period, amplitude, maximum epoch and mean magnitude from the best-fitting template (i.e. the template that minimizes the χ^2 value).

After applying the above technique, we have identified and characterized 509 RR Lyrae variables (375 ab-type and 134 c-type) in the M32 field and 630 RR Lyraes (446 ab-type and 184 c-type) in the Control field. By way of comparison, Fiorentino et al. (2012) found 416 RR Lyrae variables (314 ab-type and 102 c-type) in the same M32 field analysed herein. Fig. 4 shows a representative sample of our light curves. Tables 2–9 list the basic properties of each of these RR Lyrae variables.

In order to investigate the presence of any biases in our period-finding algorithm, we have performed extensive simulations wherein we produce ∼1000 synthetic RR Lyrae light curves with a
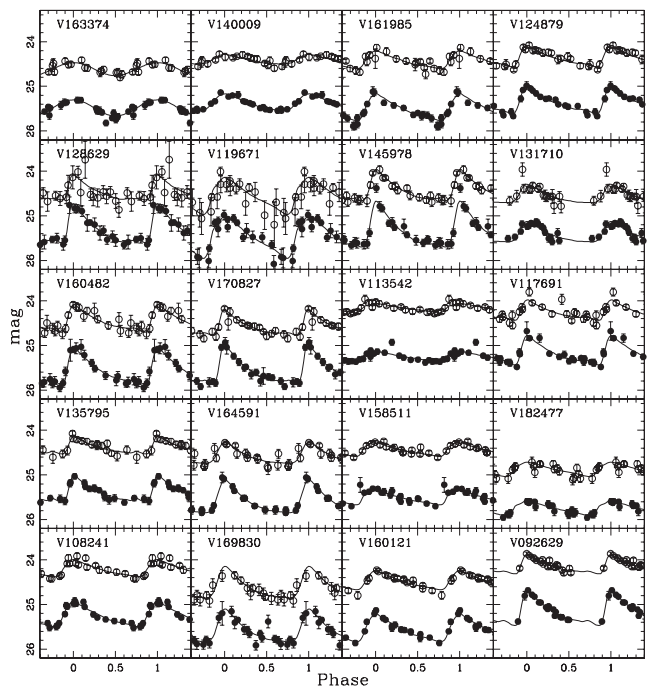
Figure 4. Example light curves of some of the RR Lyraes in our sample. The filled circles are the *F*606*W* filter data, while the open circles are in *F*814*W*. The latter have been adjusted brighter by 1 mag for illustrative purposes.

Table 2. ab-type RR Lyraes in M32 WFC1 field. The full table is available online.

Star ID	RA (J2000)	Dec. (J2000)	$\langle V \rangle$	$\langle I \rangle$	$(V - I)_{min}$	$\langle V - I \rangle$	Period (d)	*V* amplitude	*I* amplitude
69090	0 42 54.89	+40 49 36.18	25.666	25.001	0.831	0.684	0.5632	0.7199	0.4600
55439	0 42 55.13	+40 50 50.89	25.271	24.610	0.778	0.673	0.6231	0.5623	0.3681
61847	0 42 55.29	+40 51 45.40	25.399	24.790	0.637	0.610	0.5599	0.4055	0.3626
50225	0 42 55.30	+40 50 45.96	25.217	24.628	0.788	0.622	0.5827	0.8878	0.5310
54773	0 42 55.33	+40 50 39.33	25.118	24.606	0.701	0.546	0.5175	0.9801	0.6470
48015	0 42 55.35	+40 50 18.52	25.086	24.581	0.711	0.555	0.5197	1.0407	0.6680

Table 3. c-type RR Lyraes in M32 WFC1 field. The full table is available online.

Star ID	RA (J2000)	Dec. (J2000)	$\langle V \rangle$	$\langle I \rangle$	$(V - I)_{min}$	$\langle V - I \rangle$	Period (d)	*V* amplitude	*I* amplitude
55904	0 42 55.28	+40 50 41.80	25.223	24.707	0.625	0.525	0.3358	0.3853	0.2382
62969	0 42 55.37	+40 52 28.13	25.351	24.976	0.478	0.384	0.3177	0.4386	0.2929
57604	0 42 55.69	+40 49 58.02	25.223	24.741	0.620	0.492	0.3629	0.4065	0.2225
47179	0 42 55.79	+40 49 32.05	25.108	24.696	0.490	0.417	0.3836	0.3765	0.2668
62947	0 42 55.94	+40 51 42.68	25.323	24.958	0.467	0.373	0.3050	0.4364	0.2886
62331	0 42 56.01	+40 51 36.24	25.292	24.984	0.407	0.317	0.2760	0.4680	0.3216

Table 4. ab-type RR Lyraes in M32 WFC2 field. The full table is available online.

Star ID	RA (J2000)	Dec. (J2000)	$\langle V \rangle$	$\langle I \rangle$	$(V - I)_{min}$	$\langle V - I \rangle$	Period (d)	*V* amplitude	*I* amplitude
161985	0 42 45.81	+40 50 29.49	25.407	24.774	0.768	0.648	0.5709	0.6127	0.4081
124879	0 42 45.86	+40 49 15.40	25.238	24.708	0.620	0.540	0.5760	0.6285	0.4898
119671	0 42 46.02	+40 50 55.64	25.299	24.872	0.507	0.437	0.5869	0.9324	0.8322
145978	0 42 46.03	+40 50 40.41	25.160	24.752	0.592	0.445	0.4481	1.0279	0.7026
131710	0 42 46.04	+40 50 38.09	25.260	24.904	0.375	0.358	0.7845	0.4529	0.4138
160482	0 42 46.11	+40 50 32.97	25.471	24.800	0.834	0.696	0.5253	0.8770	0.6202

Table 5. c-type RR Lyraes in M32 WFC2 field. The full table is available online.

Star ID	RA (J2000)	Dec. (J2000)	$\langle V \rangle$	$\langle I \rangle$	$(V - I)_{min}$	$\langle V - I \rangle$	Period (d)	*V* amplitude	*I* amplitude
163374	0 42 45.64	+40 49 42.33	25.324	24.961	0.403	0.366	0.3409	0.3612	0.2910
140009	0 42 45.76	+40 49 35.26	25.256	24.761	0.592	0.502	0.3209	0.3690	0.2131
81800	0 42 46.41	+40 52 8.19	25.053	24.267	0.846	0.793	0.3529	0.5520	0.4156
121539	0 42 46.52	+40 49 12.69	25.193	24.692	0.524	0.502	0.3424	0.3508	0.3187
123696	0 42 46.54	+40 50 55.11	25.218	24.673	0.587	0.548	0.2986	0.3276	0.2707
178394	0 42 46.57	+40 50 29.67	25.539	25.159	0.433	0.385	0.2841	0.4103	0.3262

Table 6. ab-type RR Lyraes in Control WFC1 field. The full table is available online.

Star ID	RA (J2000)	Dec. (J2000)	$\langle V \rangle$	$\langle I \rangle$	$(V - I)_{min}$	$\langle V - I \rangle$	Period (d)	*V* amplitude	*I* amplitude
59041	0 43 27.88	+41 4 26.80	25.055	24.599	0.555	0.472	0.5134	0.7479	0.5663
80706	0 43 27.89	+41 2 14.93	25.348	24.858	0.579	0.503	0.5276	0.6531	0.5057
75357	0 43 27.93	+41 4 54.96	25.370	24.817	0.632	0.559	0.6035	0.4618	0.3593
74424	0 43 27.95	+41 4 26.71	25.264	24.756	0.648	0.527	0.5516	0.8250	0.6131
63686	0 43 27.95	+41 4 0.55	25.216	24.628	0.809	0.626	0.5834	1.0540	0.7148
90791	0 43 28.00	+41 3 5.46	25.685	24.996	0.682	0.688	0.5469	0.3511	0.3626

range of ab-type and c-type periods and amplitudes. We then input these raw synthetic light curves into RRFIT in order to determine their properties and compare them with their known values. The results are shown in Figs 5 and 6, where we plot the difference between the input and output periods (ΔP) as a function of input period. In order to estimate the errors of the individual RR Lyrae periods, we performed the following statistical test introduced in Yang et al. (2010) and also used in Yang & Sarajedini (2012). From the artificial RR Lyrae lists, we randomly draw the same number of artificial RR Lyrae stars as the observed RR Lyraes in each field [M32: 375 (RRab) and 134 (RRc); Control: 446 (RRab) and 184 (RRc)] to calculate an average ΔP value for each sample drawn. We consider the spread of a ΔP distribution as the estimate of the error. To increase its statistical significance, we iterated this sampling 10 000 times. The average spread ($\langle \sigma \rangle$) of 10 000 samples provides a realistic error for our period measurements. We applied the same method to calculate errors in the *V*-band amplitude. The resulting values of the errors are shown in Table 10. Also displayed

**Table 7.** c-type RR Lyraes in Control WFC1 field. The full table is available online.

Star ID	RA (J2000)	Dec. (J2000)	$\langle V \rangle$	$\langle I \rangle$	$(V-I)_{min}$	$\langle V-I \rangle$	Period (d)	V amplitude	I amplitude
65042	0 43 27.91	+41 4 41.46	25.173	24.839	0.421	0.340	0.3229	0.3431	0.2088
47031	0 43 27.94	+41 2 9.82	25.031	24.629	0.475	0.407	0.3033	0.3518	0.2256
57030	0 43 28.09	+41 3 25.20	25.223	24.700	0.576	0.528	0.3240	0.4322	0.3611
70608	0 43 28.29	+41 4 3.26	25.249	24.853	0.496	0.404	0.3141	0.4313	0.2836
76098	0 43 28.40	+41 4 0.59	25.440	24.845	0.663	0.600	0.2849	0.3845	0.2912
71804	0 43 28.42	+41 4 20.76	25.190	24.706	0.504	0.485	0.4015	0.2650	0.2377

Table 8. ab-type RR Lyraes in Control WFC2 field. The full table is available online.

Star ID	RA (J2000)	Dec. (J2000)	$\langle V \rangle$	$\langle I \rangle$	$(V-I)_{min}$	$\langle V-I \rangle$	Period (d)	V amplitude	I amplitude
83936	0 43 18.42	+41 5 8.04	25.314	24.737	0.773	0.602	0.5473	0.7587	0.4600
82752	0 43 18.43	+41 5 14.88	25.255	24.672	0.866	0.630	0.5550	1.0333	0.5900
99546	0 43 18.43	+41 4 33.19	25.372	24.855	0.671	0.536	0.4587	0.6070	0.3421
89174	0 43 18.51	+41 4 24.55	25.305	24.752	0.581	0.557	0.5740	0.5056	0.4549
60763	0 43 18.53	+41 4 47.27	25.208	24.532	0.725	0.679	0.6127	0.4068	0.3328
102771	0 43 18.64	+41 2 60.00	25.269	24.842	0.620	0.472	0.4868	1.2036	0.8786

Table 9. c-type RR Lyraes in Control WFC2 field. The full table is available online.

Star ID	RA (J2000)	Dec. (J2000)	$\langle V \rangle$	$\langle I \rangle$	$(V-I)_{min}$	$\langle V-I \rangle$	Period (d)	V amplitude	I amplitude
65950	0 43 18.49	+41 4 40.08	25.099	24.640	0.568	0.465	0.3337	0.3478	0.2000
103817	0 43 18.57	+41 3 7.61	25.355	24.972	0.418	0.386	0.3460	0.3824	0.3252
91215	0 43 18.78	+41 2 24.17	25.231	24.824	0.432	0.409	0.3439	0.3137	0.2731
93640	0 43 18.83	+41 4 51.84	25.347	24.807	0.634	0.547	0.3330	0.3698	0.2415
53982	0 43 18.83	+41 4 6.12	24.948	24.471	0.522	0.481	0.3692	0.2962	0.2375
91682	0 43 19.17	+41 4 34.53	25.287	24.879	0.416	0.408	0.3207	0.3438	0.3294
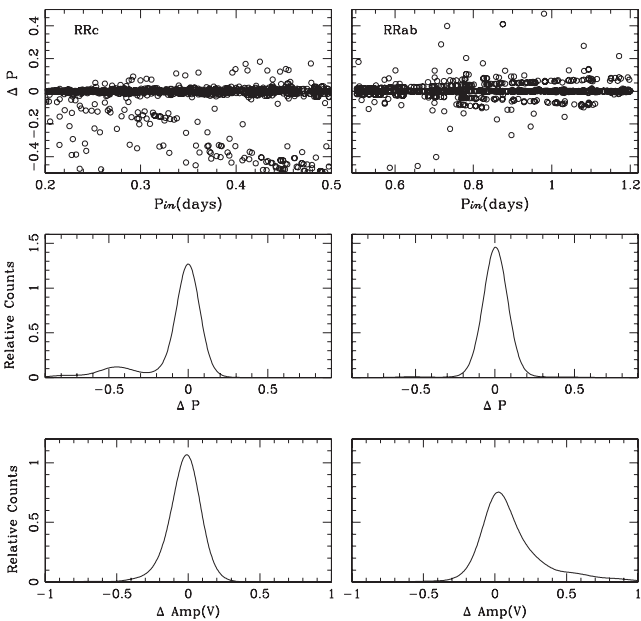
Figure 5. The results of our RR Lyrae light-curve simulations using an observing cadence appropriate for the M32 field.
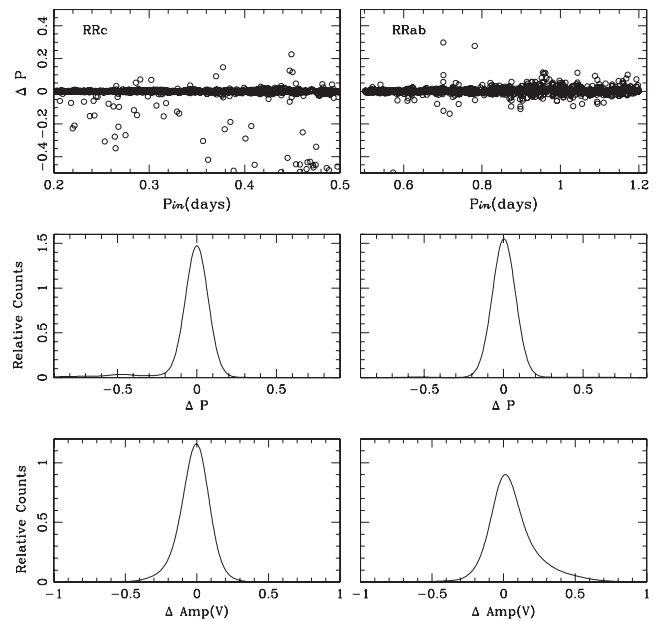
Figure 6. The results of our RR Lyrae light-curve simulations using an observing cadence appropriate for the Control field.

in this table is the fraction of simulations where the recovered period differed from the input period by less than ± 0.05 d and ± 0.1 d.

We note that the simulations reveal little or no aliasing among the RR Lyrae periods of the Control field. Even in the M32 field, where

Fig. 5 does show the signature of aliasing, the number of stars in the aliased 'bands' is a small fraction of the total number of simulations run as demonstrated by the values in Table 10. In fact, we found no significant biases in our determination of the mean periods and

Table 10. Results of the light-curve simulations.

Field	RR Lyrae type	Period error	Amplitude error	Per cent within ±0.05 d	Per cent within ±0.1 d
M32	RRab	±0.0014	±0.0084	83	96
M32	RRc	±0.0104	±0.0061	79	81
Control	RRab	±0.0008	±0.0055	94	98
Control	RRc	±0.0044	±0.0046	91	94
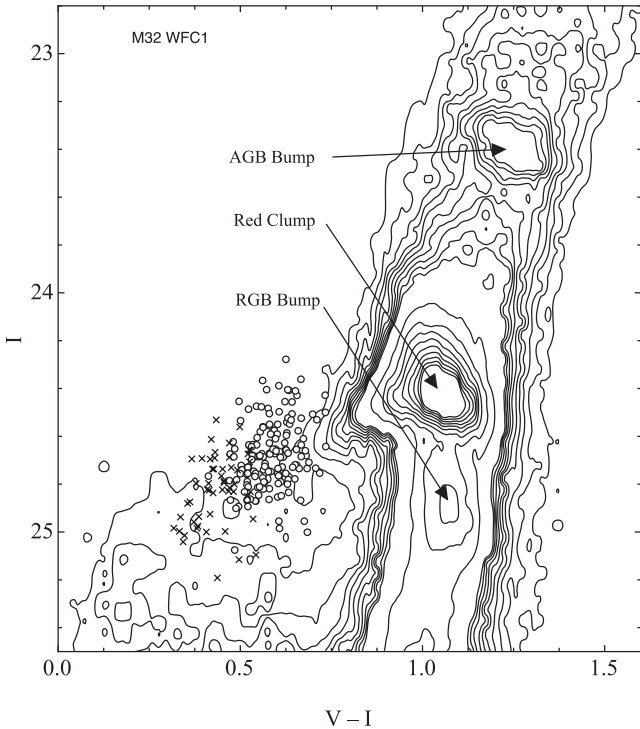
Figure 7. The CMD of stars measured on the WFC1 chip of the M32 field. The ab-type RR Lyraes are indicated as open circles, while the c-types are shown as crosses.

amplitudes as shown by the relatively small errors listed in Table 10. Hence, we assume that period aliasing does not significantly affect the results in the remainder of our analysis, which is mainly focused on the mean periods, mean amplitudes and results derived from them.

5 RR Lyrae VARIABLES IN M32

We first examine the properties of the RR Lyrae variables in M32. Figs 7 and 8 show the CMDs of the WFC1 and WFC2 chips in the M32 field. Both CMDs show a strong red giant branch (RGB), Red Clump (RC), asymptotic giant branch bump ($\approx$1 mag above the RC) and RGB bump ($\approx$0.5 mag below the RC). These features were first detected in the CMD presented by Monachesi et al. (2011), constructed from an ACS/HRC field which is entirely overlapped by our observations. Monachesi et al. (2011) showed that the CMD locations of those features indicate that the bulk of the stellar population in M32 at $\sim$2 arcmin from its centre is 8–10 Gyr old. The WFC2 CMD clearly shows more scatter, which is not unexpected given the fact that it is located closer to the centre of M32. The RR Lyrae variables are also plotted in these CMDs and occupy a region that is typical for these stars.
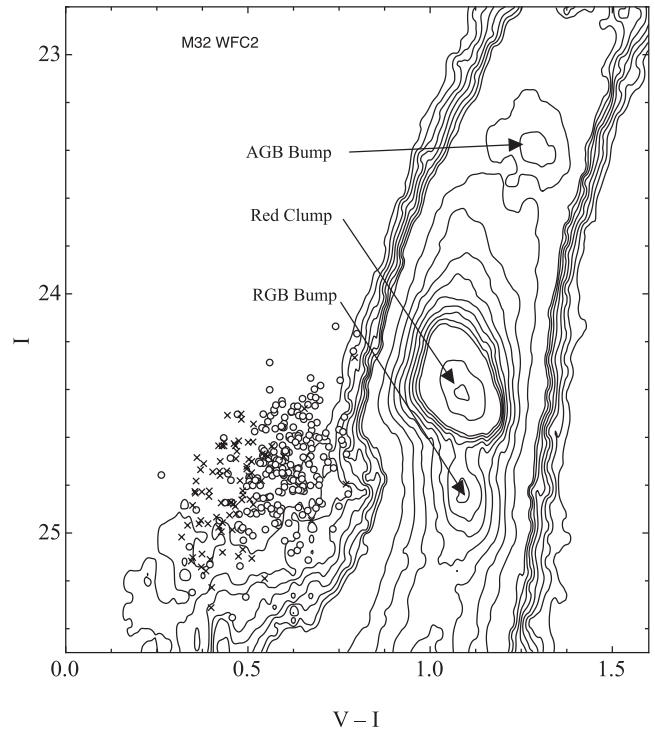
Figure 8. The CMD of stars measured on the WFC2 chip of the M32 field. The ab-type RR Lyraes are indicated as open circles, while the c-types are shown as crosses.

5.1 The radial density profile of RR Lyraes around M32

We are interested in establishing the membership of our RR Lyrae sample with regard to whether the majority of these stars belong to M32 or the background M31 population. To do so, we show the radial density distribution of these stars projected on to the major axis of M32 as compared with the RC stars in Fig. 9. The red clump stars are core-helium-burning horizontal branch stars in the same phase of evolution as the RR Lyraes. To isolate these stars, we use an I-band magnitude range of 24.2–25.2 and a colour range of 0.8–1.2. The upper panel of Fig. 9 illustrates the radial density profiles of the RC and RR Lyrae stars from the present study, where we have applied photometric completeness corrections based on the artificial star experiments described earlier. We also include the RR Lyraes from the F1 HRC field of Fiorentino et al. (2010, cross) and from Field 1 of S09 (open squares). The profiles of the RR Lyrae stars have been scaled to match the RC stars in the region outside of 150 arcsec. The dashed line in the upper panel of Fig. 9 is our adopted M31 background RR Lyrae density of 0.0077 stars arcsec^{-2} as derived from the outermost RR Lyrae point based on the observations in the present study. We note that the average density of the seven outermost points from the S09 study ($R_{\mathrm{major\,axis}} \geq 300$ arcsec) is 0.0068 ± 0.00070 stars arcsec^{-2}, which is consistent with our adopted value.

Adopting the outermost radial point as representative of the M31 background, we subtract this from the RC and RR Lyrae distributions and plot the result in the lower panel of Fig. 9 along with the M32 major axis surface brightness profile from Choi, Guhathakurta & Johnston (2002). The latter has been scaled to fit the RC profile outside of 90 arcsec. We see that the RC and RR Lyrae star radial distributions agree from $\approx$100 arcsec out to the limit of the data. These in turn are consistent with the shape of the surface brightness profile from Choi et al. (2002). In contrast, the innermost RR Lyrae
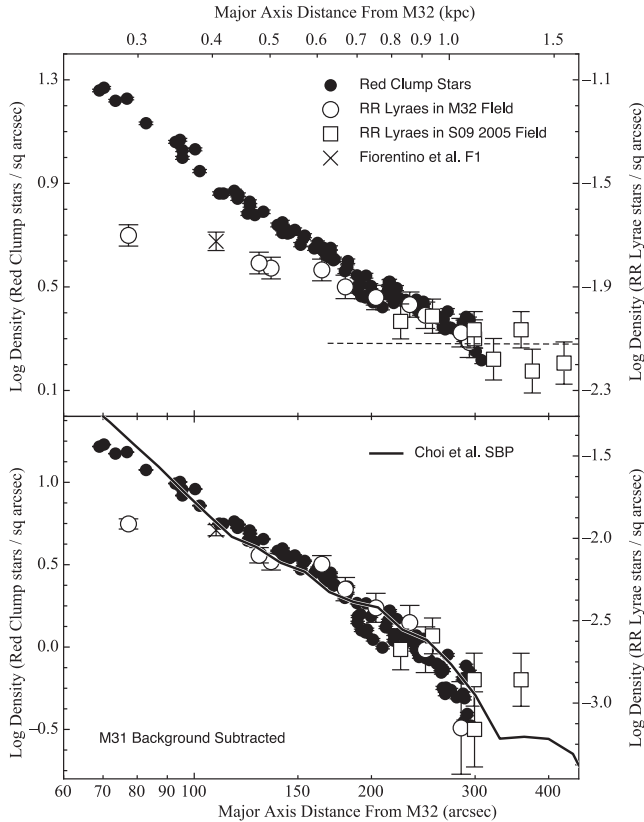
Figure 9. The radial density profiles of red clump stars and RR Lyrae variables projected along the major axis of M32. The upper panel shows the raw profiles corrected for photometric incompleteness before the subtraction of the M31 background. In addition to the red clump stars (filled circles) and RR Lyraes (open circles) from the present study, we also include the RR Lyraes from the Fiorentino et al. (2010, cross) F1 HRC field and from Field 1 of S09 (open squares). The profiles of these two populations have been scaled to match in the region outside of 150 arcsec. The upper abscissa assumes an M32 distance of 770 kpc. The dashed line is our adopted M31 background RR Lyrae level. In the lower panel, we have subtracted the M31 background density from the red clump stars and RR Lyraes and also include the M32 major axis surface brightness profile (SBP) from Choi et al. (2002) scaled to fit the red clump and RR Lyrae distribution.

point at ≈ 77 arcsec is significantly below the RC profile at that location. This is most likely a result of the fact that our detection and characterization of RR Lyraes in the inner regions of M32 has been adversely affected by the high stellar crowding. These are not accounted for in our assessment of photometric completeness and are more pronounced as the centre of M32 is approached.

As mentioned above, Fig. 9 shows that the RR Lyraes follow the RC radial profile very closely, which in turn follows the M32 surface brightness profile from Choi et al. (2002). This suggests that a significant fraction of the RR Lyraes in this ACS field belong to M32. As a result, this is evidence that M32 contains RR Lyrae variables and therefore a population older than ≈ 10 Gyr.

In order to estimate the number of RR Lyraes that likely belong to M32 in this field, we integrate the RR Lyrae radial profile in the lower panel of Fig. 9, which is the one that is background subtracted and completeness corrected. Doing this, we find 222 RR Lyraes in this field that belong to M32. This can be compared with the results of Fiorentino et al. (2012), who claimed a total of 83 RR Lyraes belonging to M32 in this field. The difference between these two estimates likely stems from two sources. First, we have identified
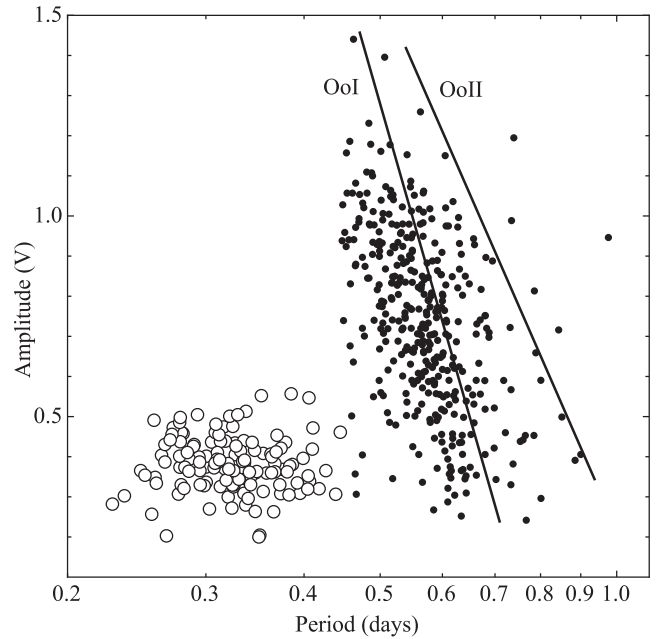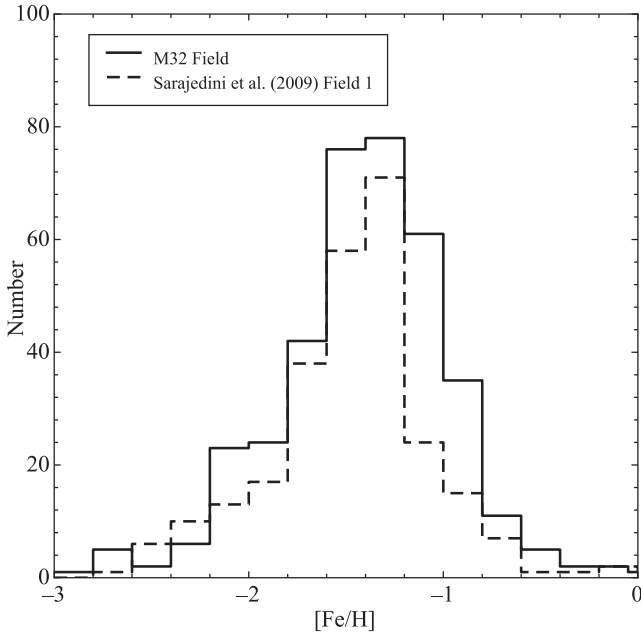
and characterized 509 RR Lyraes in the M32 field compared with 416 from Fiorentino et al. (2012) – a factor of 1.22 more objects. Secondly, the background density of M31 RR Lyraes in the present paper is approximately a factor of 1.4 lower than that assumed by Fiorentino et al. (2012) – 0.0077 stars arcsec^{-2} compared with 0.011 stars arcsec^{-2}. If we use the background density adopted by Fiorentino et al. (2012), we arrive at a total number of 71 RR Lyraes belonging to M32, which, when multiplied by a factor of 1.22, yields 87 RR Lyraes, which is close to the value of 83 quoted by Fiorentino et al. (2012). As a result, the main source of the difference between the present work and that of Fiorentino et al. (2012) with regard to the number of RR Lyraes belonging to M32 is the adopted contribution of such stars from the M31 background.

5.2 The Bailey diagram of RR Lyrae variables associated with M32

Fig. 10 shows the Bailey diagrams for the RR Lyraes in the M32 field. The ab-type RR Lyraes are shown by the filled points, while the c-type variables are plotted as open circles. The Oosterhoff I and II loci are also indicated (Clement & Rowe 2000). A comparison of these diagrams with fig. 10 of S09 suggests that the RR Lyraes in the M32 field are located slightly to the left (shorter period) of the Oosterhoff I line. We note that this field has no significant population of Oosterhoff II RR Lyraes. We return to this point in Section 6.1 below.

For the sake of completeness, we note that the mean periods of the RR Lyraes in the M32 field are $\langle P_{ab} \rangle = 0.575 \pm 0.004$ (sem) d and $\langle P_c \rangle = 0.326 \pm 0.005$ (sem) d. These are to be compared with mean periods of $\langle P_{ab} \rangle = 0.559$ d and $\langle P_c \rangle = 0.326$ d for the Oosterhoff I Galactic globular clusters (Jeffery et al. 2011).

Figure 10. The Bailey diagram for the RR Lyraes in the M32 field showing *V* amplitude on the ordinate and period in days on the abscissa. The filled circles represent the ab-type RR Lyraes, while the open circles are the c-types. The loci of ab-type RR Lyraes in Oosterhoff I and II Galactic globular clusters from Clement & Rowe (2000) are also shown.

Figure 11. The distribution of metallicities calculated using the equation from Alcock et al. (2000). The solid line represents ab-type RR Lyraes in our M32 field, while the dashed line is based on the Field 1 RR Lyraes from S09.

Figure 12. The distribution of reddenings calculated from the ab-type RR Lyraes in the M32 and control fields. The dashed line is the Gaussian fit to the points.

5.3 The metallicity of RR Lyrae variables associated with M32

We can calculate the metallicities of ab-type RR Lyraes in two ways. Using the data of Layden (2005) for 132 Galactic RR Lyraes in the solar neighbourhood, Sarajedini et al. (2006) established a relation between period and metal abundance of the form

$$[\text{Fe/H}] = -3.43 - 7.82 \log P_{\text{ab}}. \qquad (1)$$

This equation does not take into account the amplitudes of the RR Lyraes even though, as the Bailey diagrams show, there is a relation between amplitude and period for the ab-types. Including this effect, Alcock et al. (2000) gave a period–amplitude–metallicity relation of the form

$$[\text{Fe/H}] = -8.85[\log P_{\text{ab}} + 0.15A(V)] - 2.60, \qquad (2)$$

where $A(V)$ represents the amplitude in the V band. S09 suggest that if the amplitudes of the RR Lyraes are well determined, then equation (2) yields more precise metal abundances than equation (1). As a result, we will use equation (2) exclusively for the remainder of this paper.

For the 375 RRab stars in the M32 field, the solid line in Fig. 11 shows the distribution of [Fe/H] values given by equation (2). We find an average metal abundance of $\langle[\text{Fe/H}]\rangle = -1.42 \pm 0.02$ (sem) dex for these M32 RR Lyraes. The dashed line in Fig. 11 illustrates the metallicity distribution from Field 1 of S09, which is dominated by M31 RR Lyraes, where the average turns out to be $\langle[\text{Fe/H}]\rangle = -1.46 \pm 0.03$ (sem) dex. Furthermore, Fiorentino et al. (2010) find an average metallicity of $\langle[\text{Fe/H}]\rangle = -1.52 \pm 0.10$ dex in their F1 field, which is contained within our M32 field. These three average values are statistically indistinguishable to within the errors. We note also that we investigated the presence of a radial metallicity gradient among the RR Lyraes in M32 but found no evidence supporting such a gradient.

5.4 The reddening and distance to M32

The work of Guldenschuh et al. (2005) showed that the minimum light colour of ab-type RR Lyrae variables is equal to $V - I = 0.58 \pm 0.02$ mag regardless of their metal abundances and pulsation properties such as period and amplitude. Given this fact, we can calculate the reddening for each RRab variable in our sample as shown in Fig. 12. The Gaussian curve is fitted to the M32 field RR Lyraes and shows that the shape of the reddening histogram is consistent with a Gaussian distribution. The error on any given reddening value is composed of ± 0.02 mag from the Guldenschuh et al. (2005) calibration and ± 0.05 mag from the uncertainty inherent in the measurement of the minimum light colours. This latter value is taken from the results of our synthetic light-curve simulations described above. Taken together, these two errors suggest that the majority of the dispersion in the reddening distribution is attributable to errors inherent in the measurement of the RR Lyrae minimum light colour as opposed to internal reddening due to M31 and/or M32. The mean reddening for the ab-type RR Lyraes in the M32 field is $\langle E(V - I)\rangle = 0.134 \pm 0.088$ (sdm) ± 0.005 (sem) mag. We note that the Schlegel, Finkbeiner & Davis (1998) dust maps suggest a line-of-sight reddening to M32 of $E(B - V) = 0.08$ mag, which translates to $E(V - I) = 0.11$ mag (Tammann, Sandage & Reindl 2003). This is consistent with our mean $E(V - I)$ values based on the minimum light colours of the ab-type RR Lyraes, thereby corroborating the findings of previous investigators that M32 is largely free of interstellar dust (Ford, Jacoby & Jenner 1978; Impey, Wynn-Williams & Becklin 1986; Lauer et al. 1998; Corbin, O'Neil & Rieke 2001; Choi et al. 2002).

With a determination of the line-of-sight reddening and the mean metallicity of the ab-type RR Lyrae variables, we can now calculate the distance to M32. We use the RR Lyrae luminosity–metallicity relation of Chaboyer (1999): $M_V(RR) = 0.23[\text{Fe/H}] + 0.93$ mag. Adopting $E(B - V) = 0.08 \pm 0.03$ mag and $\langle[\text{Fe/H}]\rangle = -1.42 \pm 0.20$ (zero-point error in the abundance scale) dex, along with

$\langle V(\mathrm{RR})\rangle = 25.28 \pm 0.05$ (zero-point error from Sirianni et al. 2005) mag, we find $\langle (V - M)_o\rangle = 24.42 \pm 0.12$ mag for the distance to M32. This distance is consistent with a number of previous authors: 24.55 ± 0.08 mag (Tonry et al. 2001), 24.39 ± 0.08 mag (Jensen et al. 2003) and 24.53 ± 0.12 mag (Monachesi et al. 2011).

5.5 The specific frequency of M32 RR Lyraes and the ancient metal-poor population of M32

We now compute the specific frequency of RR Lyrae stars in M32. With this number we can hope to understand the ancient, metal-poor population in M32 in the context of Galactic globular clusters. Suntzeff, Kinman & Kraft (1991) define the specific frequency of RR Lyrae stars S_{RR} as the number of RR Lyrae stars N_{RR} per unit luminosity, normalized to a typical Galactic globular cluster luminosity of $M_{V_t} = -7.5$ mag:

$$S_{\mathrm{RR}} = N_{\mathrm{RR}}/10^{-0.4(M_{V_t}+7.5)} \qquad (3)$$

(following the notation of Harris 1996).

In order to compute S_{RR} for M32 RR Lyrae variables, we need to determine the luminosity of old, metal-poor M32 stars contained in the M32 ACS/WFC field. We first compute the total *B*-band magnitude of M32 in this field by integrating the *B*-band surface brightness profile of Choi et al. (2002) within the ACS/WFC field; this gives $B = 11.85$ mag. The average colour of M32 beyond one effective radius is $(B - V) = 0.88$ mag (de Vaucouleurs et al. 1991), so $V = 10.97$ mag. Combined with the distance modulus and extinction [assuming $A_V/E(B - V) = 3.315$; Schlegel et al. 1998] determined in the previous section, we find that the total *V*-band luminosity in the M32 field is $M_{V_t} = -13.7$. Monachesi et al. (2011) determined that an upper limit of ≈ 4.5 per cent of M32's mass was contained in stars with [Fe/H] < -1, or a total of ≈ 5.5 per cent of the *V*-band light from an analysis of the CMD of the RGB; Monachesi et al. (2012) determined that a lower limit of ≈ 1 per cent of M32's mass was contained in similarly metal-poor stars from analysis of the CMD near the (young) MSTOs, or a total of ≈ 1.3 per cent of the *V*-band light. We use these two values as bounds on the ancient, metal-poor starlight in the M32 ACS/WFC field; these correspond to $M_{V_t} \approx -10.6$ mag (upper limit) and $M_{V_t} \approx -9.0$ mag (lower limit) in this population. Using these luminosities, we finally derive $13 \lesssim S_{\mathrm{RR}} \lesssim 56$ for M32's RR Lyrae population (for the upper and lower limits to the mass of the ancient, metal-poor stars in M32, respectively). The lower limit is a factor of 2 larger than the value found in the much smaller ACS/HRC field by Fiorentino et al. (2010) due to our assumption of a smaller fraction of metal-poor light than assumed in that paper (5.5 per cent versus 11 per cent; the larger fraction was based on a preliminary analysis of the ACS/HRC data presented in Monachesi et al. 2011). On the other hand, the range of possible values falls within the range of Galactic globular clusters: Brown et al. (2004) find that $1 \lesssim S_{\mathrm{RR}} \lesssim 50$ at [Fe/H] ≈ -1.4 dex for Galactic globular clusters using the data presented in Harris (1996).

As discussed in Fiorentino et al. (2010), the large dispersion in S_{RR} in Galactic globular clusters with [Fe/H] < -1 dex (due to the 'second-parameter problem') means that there is no way to invert this relation to determine the *true* fraction of ancient, metal-poor stars in a population; nor do there appear to be stellar evolution models currently available that predict the population of RR Lyrae a priori (see e.g. Salaris & Cassisi 2005). The presence of RR Lyrae variables tells us that ancient, metal-poor stars are *definitely* present in M32 – a result that cannot be clearly demonstrated by existing CMDs of M32 (e.g. Monachesi et al. 2011, 2012). This in itself is a

very useful result, of course, as it shows that at least some phase of M32's evolution included metal-poor stars (Fiorentino et al. 2010, 2012).

5.6 Comparison with previous studies

The work of Fiorentino et al. (2010) imaged a field approximately 1.8 arcmin from the centre of M32, which is wholly contained within the M32 field analysed herein. They found 17 RR Lyraes in their HRC field of which 13 are recovered in our photometry. These numbers are not unexpected given the fact that our photometric completeness at this location is 88 per cent compared to 100 per cent for the Fiorentino et al. (2010) study. We have matched the RR Lyraes in common and compared the derived periods, amplitudes and magnitudes. For the periods, there is a mean difference of $\langle \Delta P\rangle = -0.0017 \pm 0.0048$ (sem) d in the sense (Fiorentino − this paper). In the case of the RR Lyrae amplitudes, we have adjusted for the difference in amplitudes expected in the *F555W* (Fiorentino et al. 2010) and *F606W* filters (present work) by decreasing the latter by 8 per cent, based on the work of Brown et al. (2004) and S09. After making this adjustment, we calculate a difference of $\langle \Delta \mathrm{Amp}(V)\rangle = 0.016 \pm 0.035$ (sem). The mean *V* magnitude difference is $\langle \Delta V\rangle = 0.016 \pm 0.029$ (sem), again in the sense (Fiorentino − Us). We see that all of these differences are quite small and well within the quoted errors.

In the case of the Fiorentino et al. (2012) RR Lyrae sample, they do not provide tables of RR Lyrae data in their paper; however, we can compare the mean properties of these stars between our study and theirs. For example, Fiorentino et al. (2012) find $\langle P_{\mathrm{ab}}\rangle = 0.55 \pm 0.07$ (sdm) and $\langle P_c\rangle = 0.32 \pm 0.04$ (sdm). In the case of the present study, our analysis yields $\langle P_{\mathrm{ab}}\rangle = 0.575 \pm 0.004$ (sem) and $\langle P_c\rangle = 0.326 \pm 0.005$ (sem). The average periods of the ab-type and c-type RR Lyraes are in good accord between the two studies. In addition, Fiorentino et al. (2012) quote a mean intrinsic *V* magnitude of $\langle V_o\rangle = 24.95 \pm 0.18$ mag. Given their adopted reddening of $E(B - V) = 0.08$, this translates to a mean apparent magnitude of $\langle V(\mathrm{RR})\rangle = 25.20$, which is in agreement with our value of $\langle V(\mathrm{RR})\rangle = 25.30 \pm 0.05$.

6 RR Lyrae VARIABLES IN M31

We now turn to the properties of RR Lyrae variables in M31, concentrating on the Control field and its implications for the M31 spheroid.

6.1 The Bailey diagram of M31 RR Lyrae variables

Fig. 13 shows the Bailey diagram for the RR Lyraes in the Control field (see Fig. 10 for the M32 population). In contrast to the M32 field, the RR Lyraes in the Control field reveal an intriguing bimodal appearance with two distinct ab-type sequences roughly bisected by the Oosterhoff type I locus. This is the first time that such bimodal behaviour has been observed among the field RR Lyrae population of M31. We investigate the significance of this phenomenon in the following sections. For now, we note, as for M32, this field does not have a significant population of Oosterhoff II RR Lyraes. As noted by S09 and Yang & Sarajedini (2012), this further underscores the general dearth of Oosterhoff II RR Lyraes in the spheroid of M31. In fact, almost all of the M31 fields observed so far – except for the Control field considered here – and M32 exhibit Bailey diagrams that resemble each other, i.e. they are all aligned with or slightly offset to shorter periods compared with the Oosterhoff I line. For
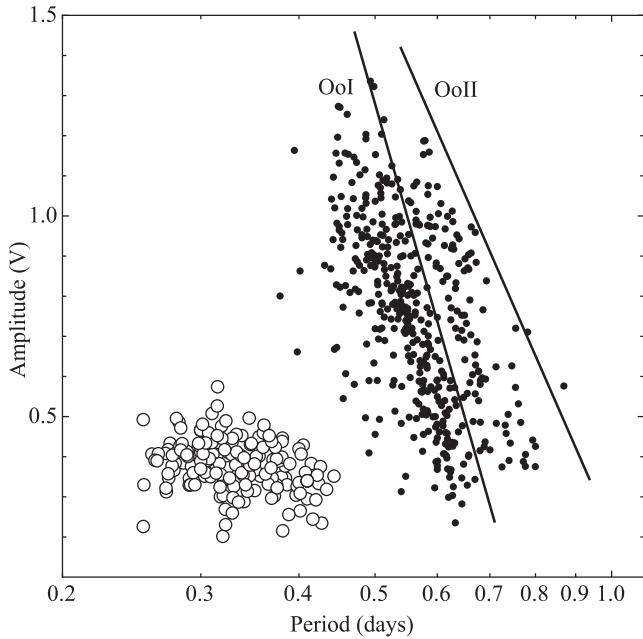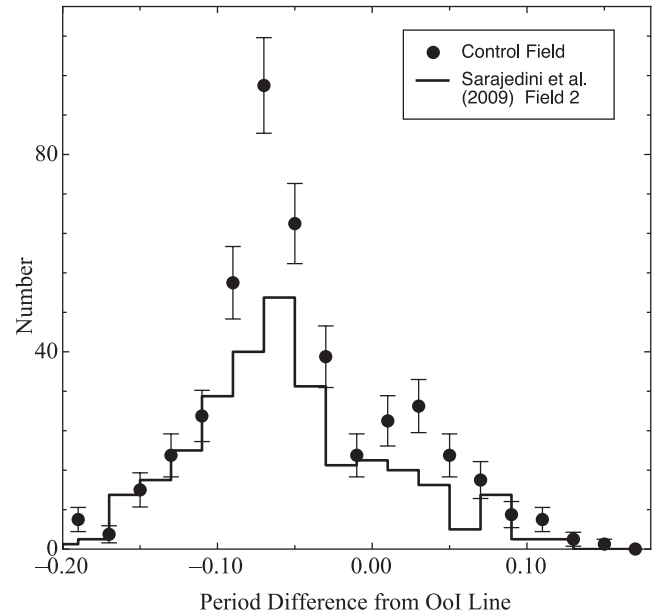
Figure 13. The Bailey diagram for the RR Lyraes in the Control field showing *V* amplitude on the ordinate and period in days on the abscissa. The filled circles represent the ab-type RR Lyraes, while the open circles are the c-types. The loci of ab-type RR Lyraes in Oosterhoff I and II Galactic globular clusters from Clement & Rowe (2000) are also shown.

Figure 14. The filled circles represent the histogram of period differences for each ab-type RR Lyrae in the Control field relative to the Oosterhoff I line shown in Fig. 13. The solid line is the histogram of period differences measured in the same way for the ab-type RR Lyraes in Field 2 of S09. The latter has been shifted horizontally by -0.03 d in order to match the dominant peaks of the two histograms.

Figure 15. The distribution of metallicities calculated using the equation from Alcock et al. (2000). The solid line represents ab-type RR Lyraes in our Control field, while the dashed line is based on the Field 2 RR Lyraes from S09.

completeness, we find $\langle P_{ab} \rangle = 0.568 \pm 0.004$ (sem) d and $\langle P_c \rangle = 0.333 \pm 0.003$ (sem) d for the Control field.

In order to investigate the robustness of the bimodality in Fig. 13, we take each ab-type RR Lyrae in the Bailey diagram and calculate its period difference relative to the Oosterhoff I line shown in Fig. 13. Since the Oosterhoff I locus roughly bisects the two subpopulations as noted above, it is a natural fiducial for this purpose. The resultant histogram of period differences is shown as the filled points in Fig. 14, wherein the solid line histogram is the Field 2 data from S09. The latter distribution has been shifted horizontally by -0.03 d in order to match the dominant peaks of the two histograms so that they can be compared in a relative manner. We see that the secondary peak present in the Control field histogram is not present in Field 2 of S09. It is also possible to compare the control field histogram shown in Fig. 14 with a single-peaked Gaussian distribution with the same mean and standard deviation via the Kolmogorov–Smirnov test. We find that there is only a 1 per cent chance that the two distributions are from the same parent population. This suggests that the bimodal appearance of the Control field Bailey diagram is likely to be genuine.

6.2 The metallicities of M31 RR Lyrae variables

Following the analysis of Section 5.3 above, the metallicity distribution function of the 446 ab-type RR Lyraes in the Control field is shown in Fig. 15. Not surprisingly, given the bimodal appearance of the Bailey diagram, these RR Lyraes exhibit a bimodal metallicity distribution with a well-pronounced peak at [Fe/H] ≈ -1.3 dex and another at [Fe/H] ≈ -1.9 dex. This is in contrast to the single-peaked distributions of the M32 field and all previous M31 fields published to date (e.g. S09; Fiorentino et al. 2010; Jeffery et al. 2011). Fig. 15 compares the Control field metallicity distribution function (MDF) with that of the RRab stars in Field 2 from S09, which has a mean abundance of $\langle$[Fe/H]$\rangle = -1.54 \pm 0.03$ (sem) dex.

Upon closer examination, it would appear that the latter may exhibit a metal-poor tail that corresponds to the metal-poor peak shown by the Control field. In any case, the bimodal appearance of Figs 14 and 15 suggests that the Control field line of sight intersects two old stellar populations with distinctly different mean metallicities. It is possible that the primary peak represents a stellar population belonging to the putative M31 spheroid, while the more metal-poor

population could have originated in a disrupted M31 dwarf satellite galaxy. If so, then the bimodal appearance of Fig. 13 represents more evidence supporting the merger and accretion history of the M31 spheroid (McConnachie et al. 2009). We note that the two metallicity peaks we find in the RR Lyraes in M31 (Fig. 15) are similar to those recently suggested by Carollo et al. (2007, 2010), which may indicate a two-phase accretion model for the creation of stellar halos (see, e.g., the review by Helmi 2008).

6.3 The reddening and distance to M31

Following the discussion in Section 5.4, we find for the Control field an average reddening of $\langle E(V-I) \rangle = 0.111 \pm 0.088$ (sdm) ± 0.004 (sem) mag (see Fig. 12). Using this value and a mean metallicity of $\langle [Fe/H] \rangle = -1.39 \pm 0.20$ dex for the Control field, we find a mean magnitude of the RR Lyraes in this field of $\langle V(RR) \rangle = 25.27 \pm 0.05$ mag. Once again adopting $E(B-V) = 0.08 \pm 0.03$, we infer a distance modulus of $\langle (V-M)_o \rangle = 24.41 \pm 0.12$ mag, which is in agreement with the result from the M32 field. We can also proceed slightly differently here by dividing the ab-type RR Lyraes in the Control field at $[Fe/H] = -1.7$ dex and calculating the distance for each group separately. We find that those with $[Fe/H] < -1.7$ dex exhibit a distance modulus of $\langle (V-M)_o \rangle = 24.43 \pm 0.12$ mag, while those with $[Fe/H] \geq -1.7$ dex have $\langle (V-M)_o \rangle = 24.41 \pm 0.12$ mag. These are essentially the same indicating that, to the level of precision with which we are able to measure it, the two stellar population components in the Control field are at the same distance. Furthermore, our distances are consistent with a number of previous values for the true distance modulus of M31, e.g. 24.44 ± 0.11 mag (Freedman & Madore 1990), 24.50 ± 0.10 mag (Brown et al. 2004) and 24.47 ± 0.07 mag (McConnachie et al. 2005).

6.4 RR Lyraes in the M31 spheroid

We can gain insight into the broader properties of RR Lyraes in M31 by examining the radial distribution of the RR Lyrae populations thus far studied. Fig. 16 illustrates these data, wherein the top panel shows the radial density distribution of M31 RR Lyraes compared with three M31 minor axis surface brightness profiles. The two inner data points come from S09 where 'halo4' represents their Field 2 and 'halo6' is their Field 1. The points designated 'M32' and 'Control' are from the present work. The halo11, halo21, halo35a and halo35b fields are the minor axis fields taken from the work of Jeffery et al. (2011), while the stream and disc points also come from Jeffery et al. (2011). The warp and outer disc fields are from the paper by Bernard et al. (2012). Next to each point, we indicate the number of RR Lyraes at that location. All of these data are based on studies that have used *HST*/ACS/WFC in order to identify and characterize the RR Lyrae variables. The solid line is the minor axis surface brightness profile from Pritchet & van den Bergh (1994, see also Brown et al. 2008) scaled to match the inner two points from S09 and the outer halo points (halo21, halo35a, halo35b). Also plotted are the minor axis surface brightness profiles from Irwin et al. (2005, thin solid line) and Gilbert et al. (2009, filled squares). We see that these three profiles agree well with each other. In order to be consistent with the minor axis surface brightness profiles, the radial positions of the inner three M31 RR Lyrae fields have been projected on to the minor axis of M31 and are plotted as such. The halo11, halo21, halo35a and halo35b points are already along the M31 minor axis.

From the top panel of Fig. 16, we note that, not surprisingly, the surface density of RR Lyrae variables in M31 drops with dis-
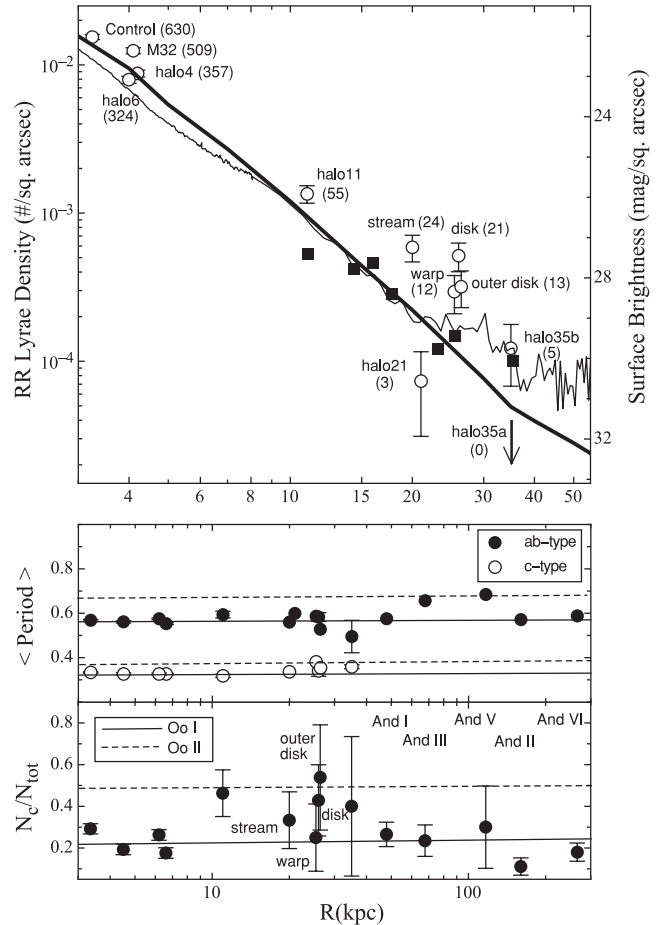

Figure 16. The upper panel shows the radial density profile of RR Lyraes in the spheroid of M31. These are referenced to the left ordinate scale. The solid line is the minor axis surface brightness profile from Pritchet & van den Bergh (1994, see also Brown et al. 2008; Courteau et al. 2011) referenced to the right ordinate axis. Also plotted are the minor axis radial brightness profiles from Irwin et al. (2005, thin solid line) and Gilbert et al. (2009, filled squares). The middle panel displays the radial trend of the mean period for the ab-type (solid circles) and c-type (open circle) RR Lyrae variables. The bottom panel is similar to the middle one except that the ratio of c-type to all RR Lyraes is illustrated as a function of radial location in the M31 spheroid. The solid lines illustrate the properties of RR Lyraes in Oosterhoff I clusters, while the dashed lines are for Oosterhoff II clusters. The properties of the Andromeda dwarf galaxies are taken from table 5 of Clementini (2010). See text for more details.

tance from its centre. The minor axis points (halo4, halo6, halo11, halo21, halo35a, halo35b) more or less follow the plotted surface brightness profile to within the errors. The stream, disc, outer disc and warp fields fall above the halo distribution, suggesting that they are enhanced in RR Lyraes above what would be expected from the halo alone. This is consistent with the conclusions of Jeffery et al. (2011) and Bernard et al. (2012) that these RR Lyraes are genuine members of these subsystems. If this is the case, then the stream, disc, outer disc and warp of M31 harbour an old stellar population, suggesting that the earliest epoch of star formation in all of these subsystems occurred at approximately the same time.

The middle panel of Fig. 16 shows the variation of mean RR Lyrae period with distance from the centre of M31 for the fields shown in the top panel as well as the data for five of the dwarf spheroidal companions of M31 taken from Clementini (2010). The
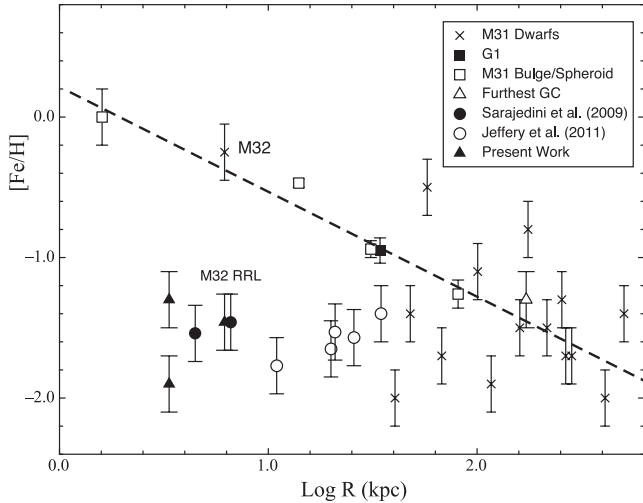
Figure 17. The radial variation of metal abundance in the M31 spheroid as originally presented by S09 (filled circles) augmented by the results of the present work (filled triangles) and those of Jeffery et al. (2011, open circles). The innermost open square represents the bulge abundance measured by Sarajedini & Jablonka (2005). The remaining open squares are the bulge/halo points from the work of Kalirai et al. (2006). The dashed line is the least-squares fit to these data with a slope of -0.75 ± 0.11. The crosses represent the dwarf galaxies surrounding M31 from the work of Grebel, Gallagher & Harbeck (2003) and Koch & Grebel (2006), whereas the abundance of M32 is taken from Grillmair et al. (1996). The filled square is the well-known massive globular cluster G1 studied by Meylan et al. (2001). The open triangle is the furthest known globular cluster in M31 discovered by Martin et al. (2006). All of these points have been scaled to an M31 distance of $(m - M)_0 = 24.43$.

mean periods of Oosterhoff I and II Galactic globular clusters are also shown as solid and dashed lines, respectively, for comparison. The upper set of solid/dashed lines refer to ab-type variables, while the lower set are for c-type variables. These lines come from the work of Jeffery et al. (2011). We see in this diagram that, with the exception of And III and And V, the rest of the M31 halo is solidly of Oosterhoff I type in terms of the mean periods of the RR Lyrae variables.

The bottom panel of Fig. 16 is similar to the middle panel except that the ratio of c-type to all RR Lyraes is plotted as a function of galactocentric distance. Once again, the M31 fields in the upper panel are included as well as the dwarf satellites from Clementini (2010). The conclusion we reached from the middle panel is also largely unchanged – to within the error bars, the M31 halo is best described as containing RR Lyraes that are most similar to Oosterhoff I Galactic globular clusters.

The reason that Oosterhoff I RR Lyraes dominate the M31 halo is related to the variation of metal abundance with radial position as discussed in S09. Fig. 17 shows an updated version of fig. 14 from S09. The metallicities for the RR Lyraes in the two fields considered herein are shown by the filled triangles, while the open circles represent the RR Lyraes considered in the study of Jeffery et al. (2011). The innermost point is the bulge metallicity from the work of Sarajedini & Jablonka (2005), while the remaining open squares are the bulge/halo points from the work of Kalirai et al. (2006) as shown in their table 3. The dashed line is the least-squares fit to the open squares with a slope of -0.75 ± 011. The other points represent the dwarf spheroidal companions to M31 (crosses; Grebel et al. 2003; Koch & Grebel 2006), the globular cluster G1 (filled

square; Meylan et al. 2001) and the furthest globular cluster in M31 (open triangle; Martin et al. 2006). Note that we have adopted the mean metallicity of M32 from the work of Grillmair et al. (1996). All of the non-RR Lyrae metallicities are based on the colours of RGB stars save for those from the study of Grillmair et al. (1996), which utilize integrated spectral indices. All of these values are based on a distance of $(m - M)_o = 24.43$ (770 kpc) for M31. In cases where an error in the metallicity is not available, we have adopted a value of ± 0.2 dex.

Metal abundance is the primary parameter affecting horizontal branch morphology among the Galactic globular clusters; this is also true in terms of the Oosterhoff dichotomy. As shown in table 2 of Clementini (2010), Oosterhoff I clusters have [Fe/H] ≈ -1.4, while those of Oosterhoff II have [Fe/H] ≈ -2.0. As Fig. 17 reveals, the halo of M31 ($R_{gc} \gtrsim 50$ kpc) has a mean metallicity that is closer to [Fe/H] ≈ -1.4 than [Fe/H] ≈ -2.0, thus corroborating its Oosterhoff I nature.

7 SUMMARY AND CONCLUSIONS

We have presented *HST*/ACS observations of two fields – one that samples the stellar populations of M32 and another dubbed 'Control' that is dominated by the spheroid of M31. Our photometry in these fields has facilitated the identification and characterization of 1139 RR Lyrae variables of which 821 are ab-type and 318 are c-type. Based on an analysis of the periods, amplitudes, magnitudes and spatial distributions of these stars, we draw the following conclusions.

(1) We find a radial gradient in the density of RR Lyraes relative to the centre of M32. This gradient is consistent with the surface brightness profile of M32, suggesting that a significant number of the RR Lyraes in this region belong to M32. This provides further confirmation that M32 contains an ancient stellar population formed around the same time as the oldest population in M31 and the Milky Way.

(2) The ab-type RR Lyraes in M32 are closer to the Oosterhoff I line in the Bailey diagram as compared to the Oosterhoff II locus exhibiting a mean metal abundance of $\langle$[Fe/H]$\rangle = -1.42 \pm 0.02$ (sem) dex.

(3) The mean reddening we measure for the M32 RR Lyraes is consistent with being due entirely to extinction within the Milky Way, reinforcing the finding of previous investigators that M32 contains little or no dust. Adopting a mean reddening of $E(B - V) = 0.08 \pm 0.03$ mag, and a relation between RR Lyrae luminosity and metallicity, we find an absolute distance modulus of $\langle (V - M)_o \rangle = 24.42 \pm 0.12$ mag for M32 and $\langle (V - M)_o \rangle = 24.41 \pm 0.12$ mag for M31 based on the Control field RR Lyrae variables.

(4) In the Control field, the Bailey diagram shows the unprecedented signature of two sequences among the ab-type RR Lyraes. When interpreted in terms of metal abundance, the primary sequence corresponds to a population of RR Lyraes with [Fe/H] ≈ -1.3 dex, while the secondary peak occurs at [Fe/H] ≈ -1.9 dex. We speculate that the primary peak represents the putative M31 spheroid, while the more metal-poor population could have originated in a disrupted M31 dwarf satellite galaxy.

(5) An examination of the global properties of RR Lyraes in the Andromeda system reveals that, with few exceptions, M31 and its satellite galaxies contain Oosterhoff type I RR Lyraes. This is likely due to the fact that the mean metal abundance of the M31 halo is more representative of Oosterhoff I Galactic globular clusters than of Oosterhoff type II clusters. Needless to say, the mere fact that

all of these systems contain RR Lyraes suggests that their earliest epoch of star formation occurred at approximately the same time.

REFERENCES

Alcock C. et al., 2000, AJ, 119, 2194
Alonso-García J., Mateo M., Worthey G., 2004, AJ, 127, 868
Aparicio A., Gallart C., 2004, AJ, 128, 1465
Bernard E. J. et al., 2012, MNRAS, 420, 2625
Brown T. M., Ferguson H. C., Smith E., Kimble R. A., Sweigart A. V., Renzini A., Rich R. M., 2004, AJ, 127, 2738
Brown T. M. et al., 2008, ApJ, 685, L121
Carollo D. et al., 2007, Nat., 450, 1020
Carollo D. et al., 2010, ApJ, 712, 692
Chaboyer B., 1999, in Heck A., Caputo F., eds, Post-Hipparcos Cosmic Candles, Vol. 237. Kluwer, Dordrecht, p. 111
Choi P. I., Guhathakurta P., Johnston K. V., 2002, AJ, 124, 310
Clement C. M., Rowe J., 2000, AJ, 120, 2579
Clementini G., 2010, in Sterken C., Samus N., Szabados L., eds, Variable Stars, The Galactic Halo, and Galaxy Formation. Sternberg Astronomical Institute, Moscow State University, p. 107
Coelho P., Mendes de Oliveira C., Cid Fernandes R., 2009, MNRAS, 396, 624
Corbin M. R., O'Neil E., Rieke M. J., 2001, AJ, 121, 2549
Courteau S., Widrow L. M., McDonald M., Guhathakurta P., Gilbert K. M., Zhu Y., Beaton R. L., Majewski S. R., 2011, ApJ, 739, 20
de Vaucouleurs G., de Vaucouleurs A., Corwin H. G., Jr, Buta R. J., Paturel G., Fouqué P., 1991, Third Reference Catalogue of Bright Galaxies. Springer, New York
Fiorentino G. et al., 2010, ApJ, 708, 817
Fiorentino G., Contreras Ramos R., Tolstoy E., Clementini G., Saha A., 2012, A&A, 539, 138
Ford H. C., Jacoby G. H., Jenner D. C., 1978, ApJ, 223, 94
Freedman W. L., 1992, AJ, 104, 1349
Freedman W. L., Madore B. F., 1990, ApJ, 365, 186
Gilbert K. M., Font A. S., Johnston K. V., Guhathakurta P., 2009, ApJ, 701, 776
Grebel E. K., Gallagher J. S., III, Harbeck D., 2003, AJ, 125, 1926
Grillmair C. J. et al., 1996, AJ, 112, 1975
Guldenschuh K. A. et al., 2005, PASP, 117, 721
Harris W. E., 1996, AJ, 112, 1487
Helmi A., 2008, A&A Rev., 15, 145
Impey C. D., Wynn-Williams C. G., Becklin E. E., 1986, ApJ, 309, 572
Irwin M. J., Ferguson A. M. N., Ibata R. A., Lewis G. F., Tanvir N. R., 2005, ApJ, 628, L105
Jeffery E. J. et al., 2011, AJ, 141, 171
Jensen J. B., Tonry J. L., Barris B. J., Thompson R. I., Liu M. C., Rieke M. J., Ajhar E. A., Blakeslee J. P., 2003, ApJ, 583, 712
Kalirai J. S. et al., 2006, ApJ, 648, 389
Koch A., Grebel E. K., 2006, 131, 1405
Kunder A., Chaboyer B., Layden A. C., 2010, AJ, 139, 415
Lauer T. R., Faber S. M., Ajhar E. A., Grillmair C. J., Scowen P. A., 1998, AJ, 116, 2263
McConnachie A. W., Irwin M. J., Ferguson A. M. N., Ibata R. A., Lewis G. F., Tanvir N., 2005, MNRAS, 356, 979
McConnachie A. W. et al., 2009, Nat, 461, 66
Martin N. F., Ibata R. A., Irwin M. J., Chapman S., Lewis G. F., Ferguson A. M. N., Tanvir N., McConnachie A. W., 2006, MNRAS, 371, 1983
Meylan G., Sarajedini A., Jablonka P., Djorgovski S. G., Bridges T., Rich R. M., 2001, AJ, 122, 830
Monachesi A., Trager S. C., Lauer T. R., Freedman W., Dressler A., Grillmair C., Mighell K. J., 2011, ApJ, 727, 55
Monachesi A., Trager S. C., Lauer T. R., Hidalgo S. L., Freedman W., Dressler A., Grillmair C., Mighell K. J., 2012, ApJ, 745, 97
Pritchet C. J., van den Bergh S., 1987, ApJ, 316, 517
Pritchet C. J., van den Bergh S., 1994, AJ, 107, 1730
Reiss A., Mack J., 2004, ISR-ACS 2004-06
Rose J., 1985, AJ, 90, 1927
Rose J. A., Arimoto N., Caldwell N., Schiavon R. P., Vazdekis A., Yamada Y., 2005, AJ, 129, 712
Rudenko P., Worthey G., Mateo M., 2009, AJ, 138, 1985
Salaris M., Cassisi S., 2005, Evolution of Stars and Stellar Populations. Wiley, Chichester
Sarajedini A., Jablonka P., 2005, AJ, 130, 1627
Sarajedini A., Barker M., Geisler D., Harding P., Schommer R., 2006, AJ, 132, 1361
Sarajedini A., Mancone C., Lauer T. R., Dressler A., Freedman W., Trager S. C., Grillmair C., Mighell K. J., 2009, AJ, 138, 184 (S09)
Schlegel D. J., Finkbeiner D. P., Davis M., 1998, ApJ, 500, 525
Sirianni M. et al., 2005, PASP, 117, 1049
Smith H. A., 1995, in Cambridge Astrophys. Ser. Vol. 27, RR Lyraes. Cambridge Univ. Press, Cambridge
Stetson P. B., 1987, PASP, 99, 191
Stetson P. B., 1994, PASP, 106, 250
Suntzeff N. B., Kinman T. D., Kraft R. P., 1991, ApJ, 367, 528
Tammann G. A., Sandage A., Reindl B., 2003, A&A, 404, 423
Tonry J. L., Dressler A., Blakeslee J. P., Ajhar E. A., Fletcher A. B., Luppino G. A., Metzger M. R., Moore C. B., 2001, ApJ, 546, 681
Trager S. C., Faber S. M., Worthey G., Gonzalez J. J., 2000, AJ, 120, 165
Worthey G., 2004, AJ, 128, 2826
Yang S.-C., Sarajedini A., 2012, MNRAS, 419, 1362
Yang S.-C., Sarajedini A., Holtzman J. A., Garnett D. R., 2010, ApJ, 724, 799

SUPPORTING INFORMATION

Additional Supporting Information may be found in the online version of this article:

Table 2. ab-type RR Lyraes in M32 WFC1 field.
Table 3. c-type RR Lyraes in M32 WFC1 field.
Table 4. ab-type RR Lyraes in M32 WFC2 field.
Table 5. c-type RR Lyraes in M32 WFC2 field.
Table 6. ab-type RR Lyraes in Control WFC1 field.
Table 7. c-type RR Lyraes in Control WFC1 field.
Table 8. ab-type RR Lyraes in Control WFC2 field.
Table 9. c-type RR Lyraes in Control WFC2 field.

Please note: Wiley-Blackwell are not responsible for the content or functionality of any supporting materials supplied by the authors. Any queries (other than missing material) should be directed to the corresponding author for the article.

This paper has been typeset from a TeX/LaTeX file prepared by the author.